Contents lists available at http://qu.edu.iq

Al-Qadisiyah Journal for Engineering Sciences

Journal homepage: http://qu.edu.iq/journaleng/index.php/JQES

Enhancement of Airfoil Performance by Rotating Cylinder

Mohammed Sadeq Kadhim[a]*, Dhafer A. Hamzah[a]

Department of Mechanical Engineering, The University of Al-Qadisiyah, Ad-Diwaniyah, Iraq.

ARTICLE INFO

Article history:
Received 18 April 2021
Received in revised form 12 June 2021
Accepted 13 June 2021

Keywords:
Airfoil
Enhancement
Rotating Cylinder
Performance
NACA6409

ABSTRACT

This study used a NACA 6409 smooth wing section. Its performance is compared to an enhanced design incorporating a revolving cylinder on the upper airfoil surface. The boundary conditions for the present work were Reynolds (10^5), and the attack angles were (0,2,4,6,8,10,12,14,16). A turbulence model was developed (SST K-), one of the aerodynamics models. This model is well-suited for sensing flow near a wall. The cylinder was evaluated at three positions (25,50,75) percent of the chord's length. The results indicated that position (25 percent C) was optimal, as it resulted in a 24.45 percent increase in lift coefficient at the angle of attack (12). And when the results were compared to those of other studies, they revealed a significant agreement.

1. Introduction

There is a growing interest in flow control, especially aerodynamics, and there are plans to increase lift and reduce airfoil resistance. Because of the adhesive effects, the wings suffer flow separation at high angles of attack, leading to a significant lift force loss and increased drag. As a result, the efforts of academics have been intensified to research and investigation the latest methods and techniques in controlling flow separation. H. Park et al.[1] presented a passive technical analysis for separating flows. The tabs were put on the airfoil's back edge, both upper and lower. An investigation was conducted experimentally by varying (height, width) of the tabs and their spacing, the Reynolds numbers ($2*10^4$, $4*10^4$, and $8*10^4$). The results indicated that the base pressure increased (drag was reduced) for all selected Reynolds numbers and that the base pressure increased by (30 %). [2, 3] Presented a study of the technique of vortex generators using different Reynolds numbers. , relied on a basic investigation, that when vortices are generated in a thicker boundary layer, the vortices transfer the high-momentum fluid to the boundary layer. This makes it thinner and has a higher resistance to reverse pressure gradient. The results showed an improvement in the airfoil performance. W.W. Huebsch et. at. [4],They view flow control as flow instability due to the viscous sublayer. The use of synthesis vortices to produce increased mixing, and absorption to obtain the correct synthesis (or a combination of the above). When the dynamic amplitude is comparable to the boundary layer height, the boundary layer state changes completely The results of this work demonstrate indicate that dynamic roughness can be employed effectively to control leading-edge separation flow in the Reynolds number range studied. the dynamic roughness is defined according to the scale of the approaching lamellar layer is entered the start of separation. The boundary layer changed earlier than the natural one. [5-10] conducted numerical and experimental investigations, or a combination of the two, on airfoils with various forms and dimples (external, internal, tennis ball shape, and teardrop shape). Experiments were conducted under various boundary conditions (Reynolds numbers, attack angles, and flow velocity). The reason behind using this technique is attributed to the dimples of various shapes generate eddies that retard or obstruct the flow's separation from the airfoil surface. These findings revealed an improvement in the airfoil's aerodynamic performance (lift and drag). Dilek F. [11] conducted a study to examine the unstable flow with increasing incidence angles and boundary conditions, Re = 103, and different angles of attack with NACA 0012 wing, the vortex pattern was calculated using the formal figure. The flux shows to be very laminar, and the boundary layers were very thick at this Reynolds number. At lower

* *Corresponding author.*
E-mail address: apk34551@gmail.com (Mohammed S. Kadhim)

https://doi.org/10.30772/qjes.v14i2.748

angles of attack, there are flux, vortex detachment, and separation. For the NACA 0012 wing, the unstable 8 ° vortex can be observed. Angles of attack usually range from 0 ° to 90 °. It is suggested that the aerodynamic forces induce an oscillation until a peak in the amplitude spectrum of the lift coefficient (Cl) is reached. At this low Reynolds number, the time-averaged streamlines, pressure, and skin friction coefficients are evaluated to see vortex development and separation from the airfoil upper surface. Pavlenko A. M. et al. [12] conducted an experimental study to investigate the evolution of hydrodynamic turbulence that resulted from the low-frequency vibrations. The results were obtained by using a low-velocity hot wire intensity meter. The results indicated that the vibrations in the wall generated disturbances in the separation region. The separation of the laminar boundary layer promoted the growth of the positive beams with the subsequent turbulence of the wall flow. Zhou Y. et al. [13] Conducted a numerical study by placing a small plate near the front edge of the airfoil. The purpose of this plate is to create an overlap between the eddies produced by the plate and the boundary layer on the airfoil surface to control the flow separation. The researchers focused on Mach number, plate length, and angle and their effect on controlling flow separation. The results indicated that Mach numbers less than (0.5) have the potential to preserve the airfoil (NACA 4405). However, Mach numbers greater than (0.5) can only obtain a slight improvement. Mahdi N. et al. [14] conducted a study to investigate delta airfoils' performance and flow characteristics with sweep angle (65˚) and coarse axial ribs. It is compared to a smooth-surface delta wing. The study investigated the effect of the ribs on (diameter, distance, and location) of vortices from the airfoil surface. The results indicated that the airtight type is positive in increasing the lift and reducing the drag. The ribs increase the flow near the upper surface except for the area near the summit. Sreejith B.K. & A. Sathyabhama [15], conducted a numerical and experimental study to verify the effect of the leading tuber with different ailerons at different angles of attack and Reynolds number 10^5. The stall occurred at an angle (12˚) in the normal wing, as observed from experimental results. The results indicated in this study that all airfoils with tuber have the same stall angle except (A2W15.5) where the stalling occurred at the angle (10˚).

By evaluating past research, we discovered a dearth of interest in studying cylinder rotation on the upper surface of the wing. Therefore, this work will focus on studying the extent of its impact on aerodynamic performance and its potential to enhance performance.

2. Describe the problem and boundary conditions

In this work, the effect of cylinder rotation on the airfoil's upper surface is considered, to improve airfoil performance. The influence of cylinder diameter was significant to obtain excellent work and satisfy the desired goal (the cylinder diameter is the same for all situations). The number of rotations of the cylinder varied according to the location. The cylinder is placed at three places that can separate the boundary layer from the length of the chord's anterior edge of an airfoil. **Table 1** shows. The boundaries of the conditions were angles of attack (0˚,2˚,4˚,6˚,8˚,10˚,12˚,14˚,16˚), flow velocity (10 m/s) and Reynolds number (10^5).

Table 1. Data & position Cylinder.

Position cylinder	N (RPM)	Diameter cylinder (cm)
25% c	124	0.54
50% c	143	0.54
75% c	172	0.54

3. Setup

3.1. Grid and computational domain

Grid and computational domain are both crucial to obtain accurate results. A two-dimensional rectangle was created (3*1.35) m, and the rectangle was 20 double the length of the chord. The height was 9 double the length of the chord. It was intended to obtain a fully developed flow. In front of the airfoil is 5 double the chord length, and behind it is 15 double length of the chord, to avoid any impact on the walls Zhong W. [16] shown in **Fig .1 a and b.**

The boundary conditions were Hare's Reynolds number (10^5) and flow velocity (10 m/s); the flow is considered to be stable, non-viscous, and incompressible. The semi-implicit method was used for the pressure-related equation computational.

The wall Y-plus parameter is a dimensionless parameter that shows the accuracy and convergence of the results, with a value less than or equal to one indicating more accurate aerodynamic results. Using the following equations, calculate Y – Plus.

$$Y = \frac{Y^{+}\mu}{\rho\, u_{*}} \quad (1)$$

Where:

$$u_{*} = \sqrt{\frac{\tau_w}{\rho}} \quad (2)$$

$$\tau_w = 0.5 C_f \times \rho \times U_{\infty}^2 \quad (3)$$

$$C_f = [2logRe - 0.65]^{-2.3}, \quad \text{For } (\text{Re} < 10^9) \quad (4)$$

$$Re = \frac{\rho c U_{\infty}}{\mu} \quad (5)$$

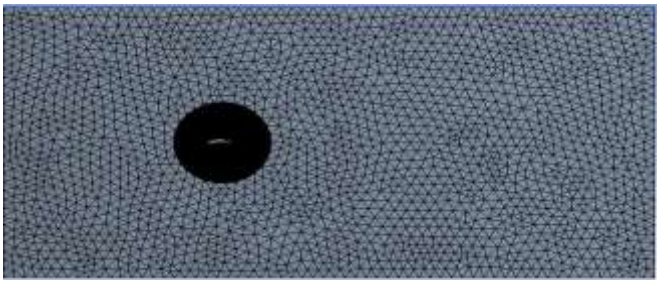

a

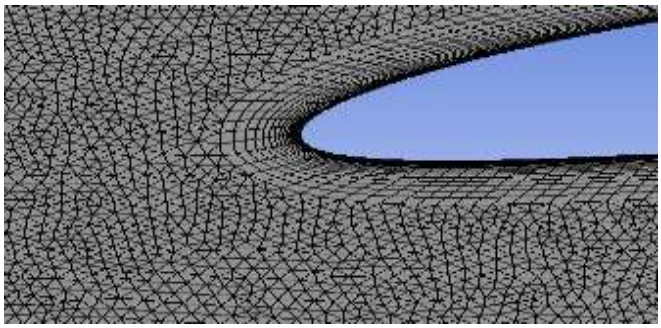

b

Figure 1. Grid for domain

3.2. Grid-independence

It is crucial to study the relationship between the mesh size and the accuracy of the solution increase in the number of cells must be investigated against variation in the convergent solution. The appropriate test methodology for the mesh independency has been adapted**,** Fish et al.[17]

The current work was carried out by selecting five meshes to check the number of cells ranged from (125536) to (633421), and this selection was implemented at the angle of attack (12˚). The convergence of lift and pull values occurred at a network consisting of cells of (517613), and the difference was almost negligible.

Table 2. Grid-independence

Iteration	Grid	Y+	C_L	C_D
923	125536	3.5	0.93419	0.03659
1846	281562	2.5	1.20001	0.04993
3218	374648	1.5	1.23986	0.05927
4509	517613	0.9	1.40609	0.06562
6340	633421	0.8	1.41352	0.06684

3.3. Turbulence model and governing equation

It is essential to find or use a disturbance model that can capture the phenomenon of transition. The current work assumes incompressible, turbulent, viscous, steady, and 2-dimensions flow with an adopted (SST k-w turbulence model), [15, 17, 18]. For the kinetic Energy of perturbation k and the specific dissipation rate w, see the equations below.

Continuity Equation

$$\frac{\partial u}{\partial x}+\frac{\partial v}{\partial y}=0 \qquad (6)$$

Momentum Equation

$$\rho u\frac{\partial u}{\partial x}+\rho v\frac{\partial u}{\partial y}=-\frac{\partial P}{\partial x}+\frac{\partial}{\partial y}\left[\mu\left(\frac{\partial v}{\partial x}+\frac{\partial u}{\partial y}\right)\right] \qquad (7)$$

$$\rho u\frac{\partial v}{\partial x}+\rho v\frac{\partial v}{\partial y}=-\frac{\partial P}{\partial y}+\frac{\partial}{\partial x}\left[\mu\left(\frac{\partial v}{\partial x}+\frac{\partial u}{\partial y}\right)\right] \qquad (8)$$

SST K-ω Turbulence model

$$\frac{\partial}{\partial t}(\rho k)+\frac{\partial}{\partial x_i}(\rho U_i k)=\tilde{P}_k-\beta^*\rho k\omega+\frac{\partial}{\partial x_i}\left[(\mu+\sigma_k\mu_t)\frac{\partial k}{\partial x_1}\right] \qquad (9)$$

$$\frac{\partial}{\partial t}(\rho\omega)+\frac{\partial}{\partial x_i}(\rho U_i\omega)=\alpha\rho S^2-\beta\rho\omega^2+\frac{\partial}{\partial x_i}\left[(\mu+\sigma_\omega\mu_t)\frac{\partial\omega}{\partial x_i}\right]+2(1-F_1)\rho\sigma_{\omega2}\frac{1}{\omega}\frac{\partial k}{\partial x_i}\frac{\partial\omega}{\partial x_i} \qquad (10)$$

Where: β* is 0.09, and $\sigma_{\omega2}$ is 0.856. F1 is the blending function, S is an invariant measure of the strain rate. In (k-ε model), the blending function equals zero when it is away from the surface, but in (k-ω model), it is one inside the boundary layer Menter et al. [19]. $\tilde{P}_k$, definition production limiter, the purpose of its use in the SST Model is to eliminate or prevent the accumulation of disturbances that occur in stagnation areas. Calculate all other constants through a combination of (k-ω) and (k-ε) models via $\alpha, \sigma_\omega, \sigma_k, etc$. Menter et al. [19, 20].

4. Results and Discussion

The study conducted a numerical analysis to investigate the problem in the flow control due to a cylinder placed on the upper surface of the airfoil with a fixed diameter of (0.54 cm), at different positions (25%, 50%, 75%) the length of the line from the front edge of the airfoil where the velocity of free flow was (10 m/s).

4.1. Validation

To determine the validity and convergence of current search results. Lift coefficients were calculated at various angles of attack (0° to 10°), then compared with those obtained in previous research E.N. Garcia et al. [21] Shown in **Fig. *2*** The study conditions under which the current research was conducted were similar to those used in previous studies. One of the most critical conditions is NACA***6409***, which is the same used in current research. There was a difference between the study previous and the current study, (the different circumstances of the two studies). found an acceptable error rate at an angle of attack (*10*°) of (*1.46*%).

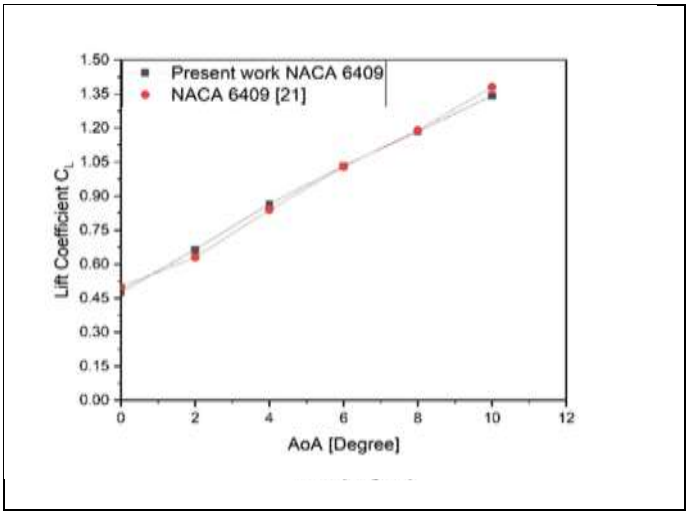

Figure 2. Lift Coefficients of the present research and researcher [8] with the Angle of Attack

4.2. Lift and Drag

Lift on an airfoil is often caused by the angle of attack and the form of the airfoil. To ensure the airfoil deflects the incoming air, the airfoil at an angle that produces a force the airfoil in the opposite direction of deflection was oriented. Moreover, aerodynamic force, is classified as lift and drag. A lift can be produced on many foil shapes, but the cambered airfoils can do so even at zero attack angles Sharma et al. [22]. From **Fig .3-a,** is observed that the lift coefficient of the smooth airfoil starting from a value higher than zero, and this proves the hypothesis above about the zero attack angle and its output for the lift coefficient. As shown **Fig. 3-a**, it can be seen that the best lifting coefficient is at the position (25%c) where the percentage of improvement was in the lift coefficient (24.45%), and this is owing to the cylinder's position and its critical function in delaying the boundary layer's separation process. **Fig. 3-b,** is shown the airfoil behavior is illustrated in relation to the drag coefficient, demonstrating that an increase in the angle of attack results in an increase in the drag coefficient. However, the proportions ranged in increasing the drag coefficient according to the effect of the cylinder position at the other positions.

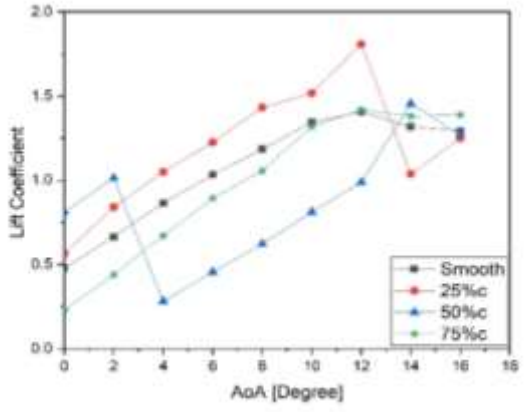

a

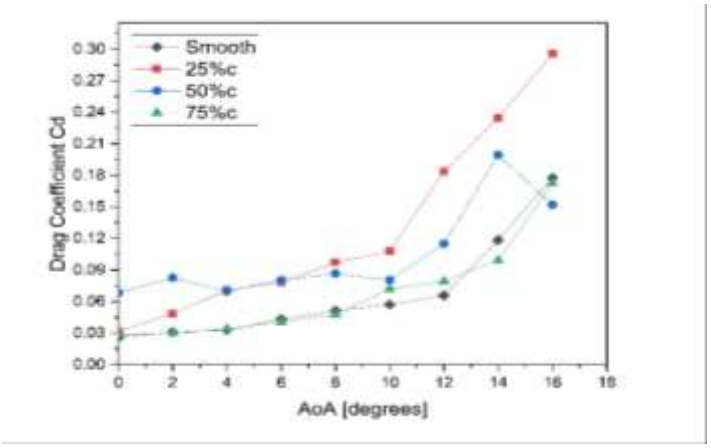

b

Figure 3. Lift & Drag coefficients with angles of attack

4.3. Velocity Contours

the area of separation of the flow from the airfoil surface, can be possibly determined, it is also possible to observe the effect of the position of the cylinder on the performance of the aileron (delaying the separation process). In **Fig. 4-a,** the separation in the airfoil is observed to be smooth at angle 12˚; from the gradient, see the separation area, as shown in **Fig. 4-a**.

Fig. 4-b explains the velocity distributions in the airfoil with the cylinder at the position (25%c). Note that the process of re-bordering the boundary layer by adhesion to the upper surface of the airfoil, which explains the increase in the lift coefficient at the angle of attack (12˚).

Fig. 4-c shows the cylinder at the position of (50%c), from the gradation of colors, see process of separation of the flow occurred early and before the cylinder. The position of the cylinder becomes ineffective inflow.

Fig. 4-d represents the velocity trends of the cylinder at (75%c). Through the results and contour, it is found that the cylinder is in the area of separation. Thus, the flow cannot be re-adhered at the airfoil surface which becomes utterly ineffective.

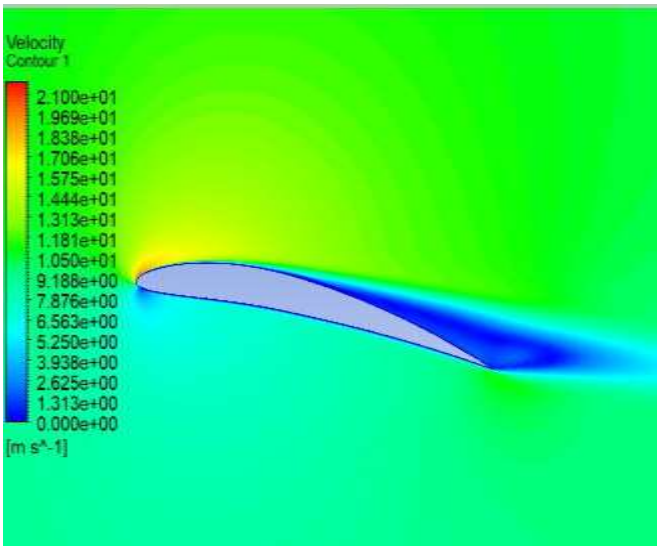

a

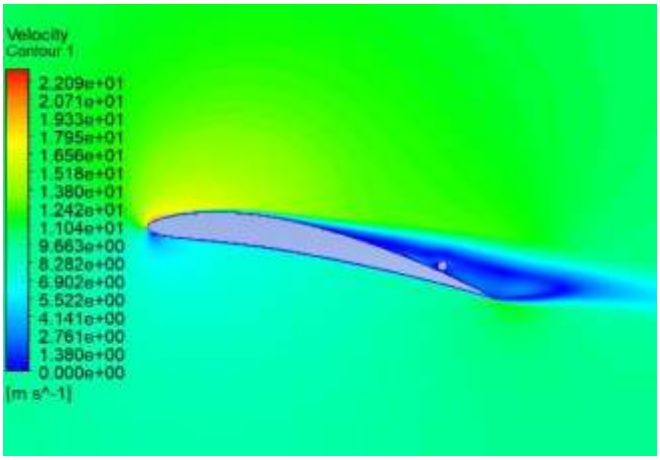

b

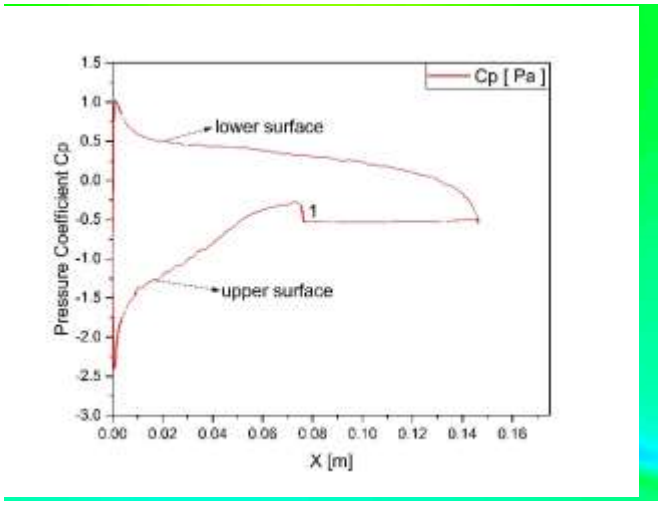

c

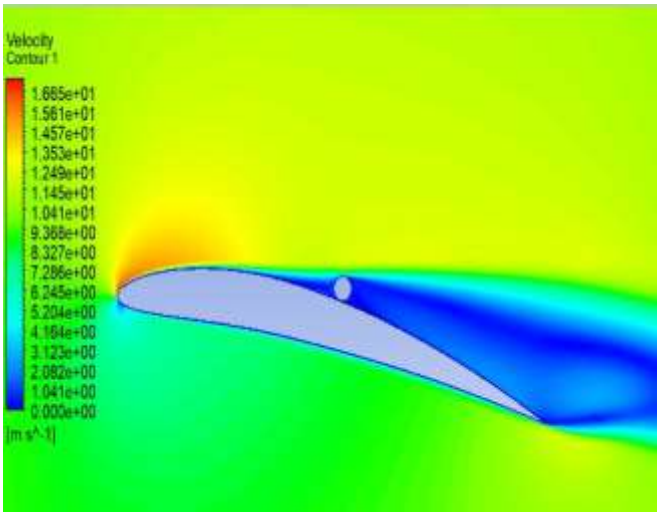

d

Figure 4. Velocity contours

4.4. Pressure Coefficient

Fig. 5 represents the air pressure coefficient on the NACA 6409 airfoil were (**Fig. 5-a**) the smooth airfoil, (**Figs-b, c, d**) for the modified airfoil, at the angle of attack (12˚). where the negative value indicates the pressure factor on the upper surface of the wing. The positive value represents the pressure coefficient on the lower surface of the wing. The results obtained indicate that the more negative the pressure coefficient on the upper surface, the higher the lift coefficient. All of the above is based on Bernoulli's principle. In **Fig. 5-b**, two locations (1 and 2) change the shape of the curve as a result of the cylinder's action on the wing surface at 25% °C. In **Fig. 5-c,** it shows the extent of the effect of the cylinder rotation at a position (25%). A change occurred in the shape of the lower curve at region (1), which represents the upper surface of the airfoil. The reason for the change is the effect of the cylinder rotation. **Fig. 5-d**, where the cylinder position is 75% c. The curve is similar to that of the smooth airfoil, when compared to **Fig. 5-a**, the result indicates, that there is no effect of cylinder rotation on the flow in position 75% c .

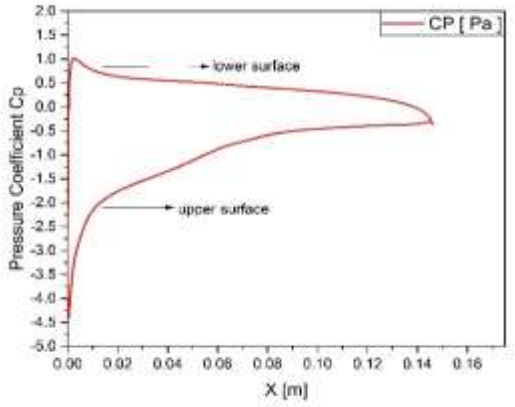

a

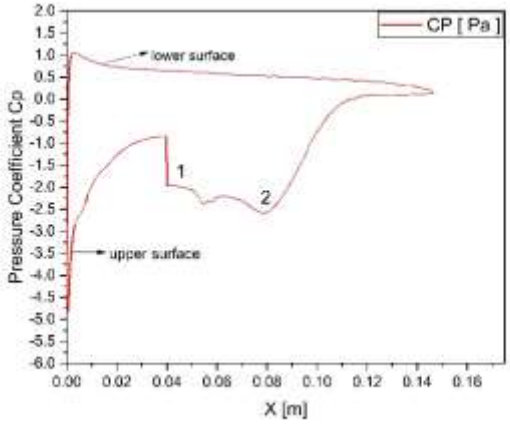

b

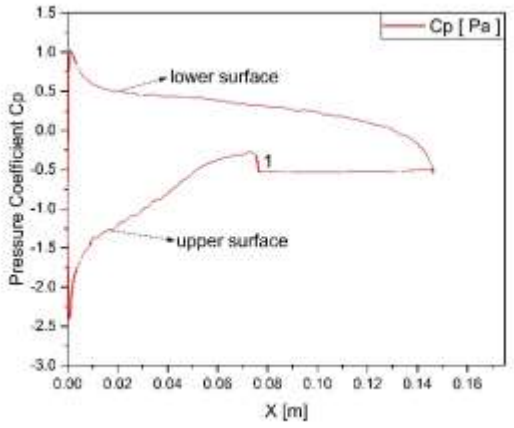

c

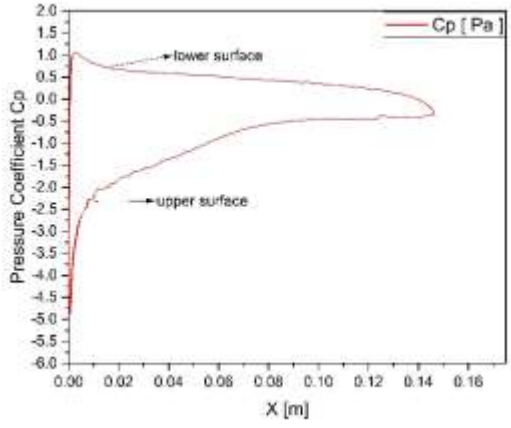

d

Figure 5. Pressure coefficient with position

5. Conclusions

A numerical study was performed on the airfoil (NACA 6409) to investigate aerodynamic performance with and without cylinder rotation on the airfoil's upper surface. Three positions of the cylinder (25%,50%,75%) were chosen from the front edge of the airfoil.

The results showed the following:

1- There is a difference in the coefficient of lift and drag values using roller rotation technology and without roller rotation on the wing's upper surface (NACA6409). This means that the lift coefficient increases with the increase in the angle of attack due to the rotation of the cylinder and the resulting pressure difference around the airfoil**.** The lift coefficient reaches its maximum value at an angle (12), and the stall angle occurs at an angle (14), the angle at which the boundary layer separated. as shown **Fig .6**. Velocity streamlines

2- The rate of increase in lift coefficient was (24.45%) position (25%). At the location of the cylinder (50%), there was no significant improvement in aerodynamic characteristics despite the increase in the lift coefficient for the angles (0˚, 2˚). After these angles, an early separation occurred at an angle of attack (4), and this is entirely undesirable. The site (75%) has a slight increase in the lift coefficient of (3.7 %).

3- Lift coefficient increases with increasing angle of attack in case the rotation of cylinder is presence or not. From the results discussed, the site (25%) is the best in terms of optimization used in this work.

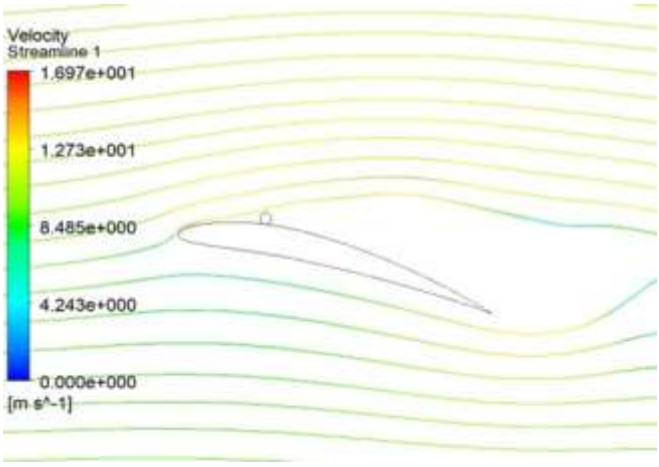

Figure 6 Velocity streamlines contour at an angle of attack (14°)

.REFERENCES

[1] H. Park, D. Lee, W.-P. Jeon, S. Hahn, J. Kim, J. Kim, J. Choi, H. Choi, Drag reduction in flow over a two-dimensional bluff body with a blunt trailing edge using a new passive device, Journal of Fluid Mechanics, 563 (2006) 389.

[2] O.M. Fouatih, M. Medale, O. Imine, B. Imine, Design optimization of the aerodynamic passive flow control on NACA 4415 airfoil using vortex generators, European Journal of Mechanics-B/Fluids, 56 (2016) 82-96.

[3] C.M. Velte, M.O.L. Hansen, D. Cavar, Flow analysis of vortex generators on wing sections by stereoscopic particle image velocimetry measurements, Environmental Research Letters, 3(1) (2008) 015006.

[4] W. Huebsch, P. Gall, S. Hamburg, A. Rothmayer, Dynamic roughness as a means of leading-edge separation flow control, Journal of aircraft, 49(1) (2012) 108-115.

[5] E. Livya, G. Anitha, P. Valli, Aerodynamic analysis of dimple effect on aircraft wing, International Journal of Mechanical, Aerospace, Industrial, Mechatronic and Manufacturing Engineering, 9(2) (2015).

[6] M. Prasath, S.I. Angelin, Effect of dimples on aircraft wing, Global Research and Development Journal for Engineering, 2(5) (2017) 234-242.

[7] H. Sedighi, P. Akbarzadeh, A. Salavatipour, Aerodynamic performance enhancement of horizontal axis wind turbines by dimples on blades: Numerical investigation, Energy, 195 (2020) 117056.

[8] Y. Sowmyashree, D. Aishwarya, S. Spurthy, R. Sah, B. Pratik, H. Srikanth, R. Suthan, Study on effect of semi-circular dimple on aerodynamic characteristics of NACA 2412 airfoil, in: AIP Conference Proceedings, AIP Publishing LLC, 2020, pp. 030009.

[9] A.J. Stolt, A.H. Ullah, J. Estevadeordal, Study of Leading-Edge Dimple Effects on Airfoil Flow Using Tomographic PIV and Temperature Sensitive Paint, Fluids,

4(4) (2019) 184.

[10] Y. Zhao, H. Lu, Y. Sun, Experimental Studies of Dimpled Surface Effect on the Performance of Linear Cascade under Different Incidence Angles, Procedia CIRP, 56 (2016) 137-142.

[11] D.F. Kurtulus, On the unsteady behavior of the flow around NACA 0012 airfoil with steady external conditions at Re= 1000, International journal of micro air vehicles, 7(3) (2015) 301-326.

[12] A. Pavlenko, M. Katasonov, V. Kozlov, A. Dovgal, Generation of localized disturbances by surface vibrations behind the ledge in the laminar flow, in: AIP Conference Proceedings, AIP Publishing LLC, 2017, pp. 030097.

[13] Y. Zhou, L. Hou, D. Huang, The effects of Mach number on the flow separation control of airfoil with a small plate near the leading edge, Computers & Fluids, 156 (2017) 274-282.

[14] N.-A. Mahdi, O. Nematollahi, K.C. Kim, Effects of coarse riblets on air flow structures over a slender delta wing using particle image velocimetry, Chinese Journal of Aeronautics, 32(6) (2019) 1367-1379.

[15] B. Sreejith, A. Sathyabhama, Experimental and numerical study of laminar separation bubble formation on low Reynolds number airfoil with leading-edge tubercles, Journal of the Brazilian Society of Mechanical Sciences and Engineering, 42(4) (2020) 1-15.

[16] W. Zhong, T. Zhang, T. Tamura, CFD Simulation of Convective Heat Transfer on Vernacular Sustainable Architecture: Validation and Application of Methodology, Sustainability, 11(15) (2019) 4231.

[17] F.E. Fish, J.M. Battle, Hydrodynamic design of the humpback whale flipper, Journal of morphology, 225(1) (1995) 51-60.

[18] H. Shah, S. Mathew, C.M. Lim, Numerical simulation of flow over an airfoil for small wind turbines using the $$\gamma-{\text {Re}} _ {\theta} $$ γ-Re θ model, International Journal of Energy and Environmental Engineering, 6(4) (2015) 419-429.

[19] F.R. Menter, M. Kuntz, R. Langtry, Ten years of industrial experience with the SST turbulence model, Turbulence, heat and mass transfer, 4(1) (2003) 625-632.

[20] F. Menter, R. Langtry, S. Völker, Transition modelling for general purpose CFD codes, Flow, turbulence and combustion, 77(1-4) (2006) 277-303.

[21] E.N. Garcia, V. Durgesh, H. Johari, Experimental Study of NACA Symmetric and Camber Airfoils at Low Reynolds Numbers, in: 55th AIAA Aerospace Sciences Meeting, 2017, pp. 0771.

[22] A. Sharma, S.G. Kumar, D.N.G. Ratha, Evaluation of Flow Behavior around an Airfoil Body, 2012.